Individually addressable epitaxial ferroelectric nanocapacitor arrays with near Tb inch^{-2} density

WOO LEE[1,3]*, HEE HAN[2], ANDRIY LOTNYK[1], MARKUS ANDREAS SCHUBERT[1], STEPHAN SENZ[1], MARIN ALEXE[1], DIETRICH HESSE[1], SUNGGI BAIK[2] AND ULRICH GÖSELE[1]

[1]Max Planck Institute of Microstructure Physics, Weinberg 2, D-06120 Halle, Germany
[2]Department of Materials Science & Engineering, Pohang University of Science and Technology, San 31, Hyoja-dong, 790-784 Pohang, Korea
[3]Korea Research Institute of Standards and Science (KRISS), Yuseong, 305-340 Daejon, Korea
*e-mail: woolee@kriss.re.kr

Published online: 15 June 2008; doi:10.1038/nnano.2008.161

Ferroelectric materials have emerged in recent years as an alternative to magnetic and dielectric materials for nonvolatile data-storage applications[1–5]. Lithography is widely used to reduce the size of data-storage elements in ultrahigh-density memory devices[6–9]. However, ferroelectric materials tend to be oxides with complex structures that are easily damaged by existing lithographic techniques, so an alternative approach is needed to fabricate ultrahigh-density ferroelectric memories. Here we report a high-temperature deposition process that can fabricate arrays of individually addressable metal/ferroelectric/metal nanocapacitors with a density of 176 Gb inch^{-2}. The use of an ultrathin anodic alumina membrane as a lift-off mask makes it possible to deposit the memory elements at temperatures as high as 650 °C, which results in excellent ferroelectric properties.

Research into new ferroelectric memory devices generally involves the use of a scanning probe microscope to write data to, and read data from, data-storage elements[10]. Data are written by applying a voltage pulse to the tip of the microscope to switch the ferroelectric polarization of the memory element. To read the data the microscope is operated in either the piezoresponse mode[11] or the recently developed nonlinear dielectric mode[12]. Storage densities of 1 Tb inch^{-2} or higher can, in principle, be achieved by using piezoresponse force microscopy (PFM) to write data onto a uniform storage medium, but this approach suffers from several drawbacks. First, the domain size on the surface of the ferroelectric storage medium depends on the nature of the writing element (that is, the tip) and the voltage[13]. Second, there are stability problems due to the possibility of domains merging or collapsing[14]. Finally, there are variations in the size of the contact area between the tip and the storage medium, which leads to variations in the domain size.

Patterning the surface into an array of individually addressable metal/ferroelectric/metal (MFM) nanocapacitors has a number of advantages. Because the individual memory elements storing the bits of data are physically separate, the electric field distribution is much more localized (see Suppementary Information, Fig. S1), crosstalk is reduced, and there are no internal depolarization fields due to the symmetric structure.

Extended arrays of ferroelectric $Pb(Zr_{0.20}Ti_{0.80})O_3$ (PZT) nanostructures or MFM nanocapacitors were deposited on Pt/MgO(100) and Nb-doped $SrTiO_3$(100) single-crystal substrates by pulsed laser deposition (PLD) of PZT material through ultrathin anodic aluminium oxide (AAO) masks (Fig. 1a). Self-ordered ultrathin AAO masks (Fig. 1b) were fabricated by anodization of aluminium (see Methods and Supplementary Information, Fig. S2). The AAO mask was first placed on the substrate of choice. PZT was subsequently deposited at an elevated growth temperature (650 °C) by PLD. Owing to the high aspect ratio of the AAO mask, the PLD process has to be performed at low oxygen pressures (to enhance the energy of the impinging species) and at high temperatures, usually higher than 400 °C (to increase the surface mobility of the adsorbed species in order to prevent them closing the top opening of the porous mask). Following the lift-off process to remove the AAO mask, the structural and ferroelectric properties of the resulting PZT nanostructures were characterized using scanning electron microscopy (SEM), transmission electron microscopy (TEM), synchrotron X-ray diffraction and PFM. For SEM micrographs, we partly removed the oxide mask in order to visualize both the mask and the resulting PZT nanostructures (Fig. 1c). The average size and pitch of the PZT nanostructures, 64 nm and 104 nm, respectively, are identical to the pore size and the interpore distance of the oxide mask used during PLD (see Supplementary Information, Fig. S3).

In comparison to conventional resist-based patterning or electron-beam techniques, the present AAO-based nanofabrication process is a generic and unique approach for direct epitaxial growth of nanostructures where high temperatures are required for the deposition onto the substrate. The subsequent lift-off process is solvent-free, so very sensitive materials can be processed without the risk of cross-contamination, etching or mechanical damage, all of which could be of serious concern, particularly in the manufacture of ferroelectric nano-objects, where severe lattice damage to sidewalls results in degradation of their ferroelectric properties[9,15]. These advantages, as well as the low cost and accessibility of the process, make the present technique very suitable for fabrication of large-area periodic patterns. It enables the

© 2008 Macmillan Publishers Limited. All rights reserved.

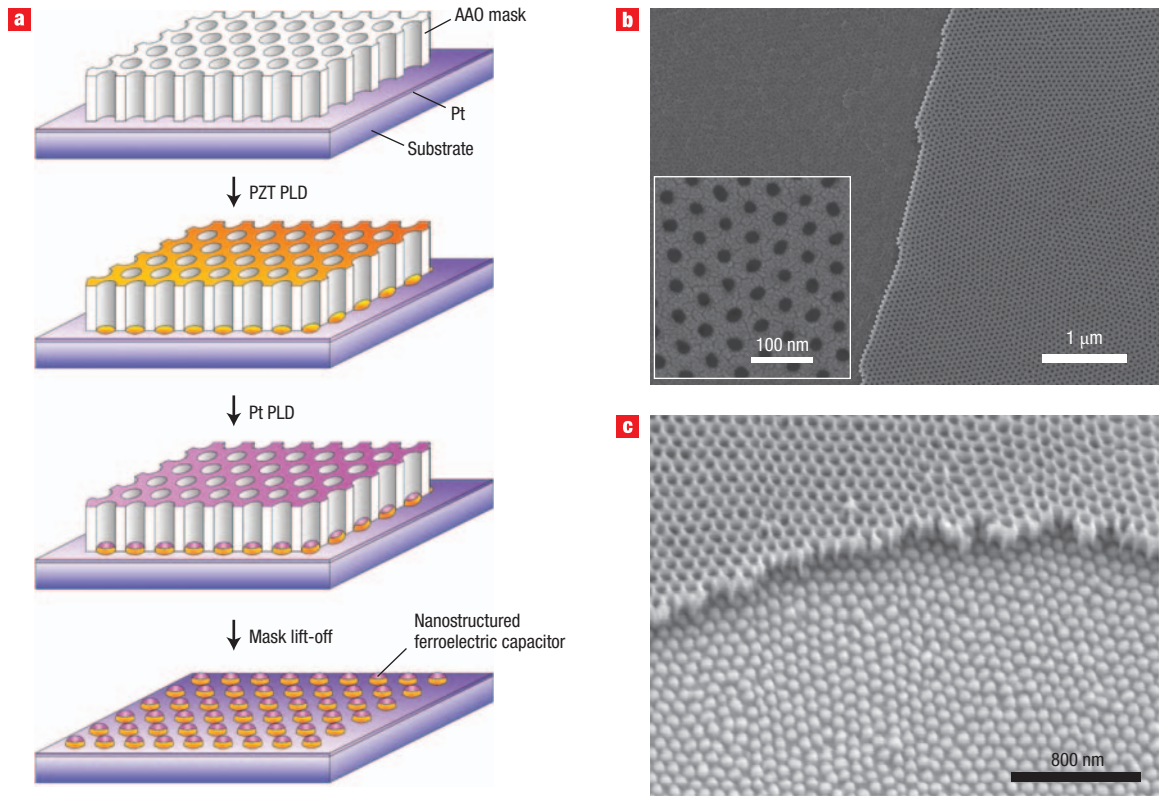

Figure 1 Fabrication of the nanocapacitors. a, Schematic showing the pulsed laser deposition of the ferroelectric material PZT through an ultrathin AAO mask onto a Pt layer on a substrate, followed by the deposition of Pt and then lift-off of the mask to leave an extended array of nanocapacitors. **b**, Typical SEM micrograph of the ultrathin AAO mask. Inset: magnified view. **c**, As-prepared PZT nanoisland array with the AAO mask visible at the top of the image. The nanoisland density ρ can be estimated by assuming that the pores are arranged hexagonally: we find that $\rho = (2 \times 6.45/\sqrt{3}D_{int}^2) \times 10^{14}$ inch^{-2}, where D_{int} is the interpore distance (in nm). The densities are calculated to be 176 Gb inch^{-2} for a H_2SO_4-AAO mask ($D_{int} = 64$ nm) and 68 Gb inch^{-2} for an $H_2C_2O_4$-AAO mask ($D_{int} = 104$ nm).

realization of two-dimensional (2D) extended arrays (typically of a scale greater than cm^2) of structurally well-defined nanostructures, with properties that can be accessed by conventional characterization methods for bulk materials, such as X-ray diffraction, superconducting quantum interference device measurements, and so on. Additionally, complex structures such as patterned epitaxial multilayers and capacitors are easily achievable.

The average height of the PZT nanoislands was 40 nm (Fig. 2a). Electron diffraction analyses indicated epitaxial growth on the Pt/MgO(100) substrate (Fig. 2b,c; see also Supplementary Information, Fig. S4, for an example of Nb-doped STO(100) substrate). High-resolution TEM (HRTEM) analyses confirmed both the epitaxial growth and the high quality of the sidewalls (Fig. 2d), which could not be accomplished by conventional top-down nanofabrication approaches based on focused ion beam (FIB) or dry-etching techniques[7,8]. The multilayer structures of MFM nanocapacitors with a Pt/PZT/Pt stacking configuration on MgO(100) are shown in Fig. 2e,f.

Recently, we reported the use of a gold nanotube membrane as a lift-off mask for patterning La-doped $Bi_4Ti_3O_{12}$ or $Pb(Zr_{0.40}Ti_{0.60})O_3$ nanodots with a typical lateral size greater than 120 nm (refs. 16 and 17). Although this generic approach is very effective for generating nanostructures, the deposition had to be carried out at room temperature because of the thermal instability of the stencil. For ferroelectric nanostructures in particular, a high-temperature post-annealing step has then to be performed in order to crystallize them[16,17]. This two-step approach is not feasible for creating sub-100-nm epitaxial PZT nanostructures and capacitors (see Supplementary Information, Fig. S5).

The ferroelectric properties of the PZT nanostructures were investigated by PFM. Hysteresis loops were obtained at 25 kHz. Typical ferroelectric hysteresis curves measured from a single ferroelectric nanodot and an MFM nanocapacitor, respectively, are presented in Fig. 3. Each nanoisland shows a well-developed ferroelectric hysteresis curve, as determined by PFM, with a coercive voltage of about 0.8 V and an effective remanent piezoelectric constant of about 100 pm V^{-1}, comparable to the theoretical values. These high values and the a–c domain structure revealed by the PFM pattern (Fig. 3c) on nanostructures without top electrodes suggest a rather low level of strain in the epitaxial PZT structures. The sharp switching and the squareness of the hysteresis loop indicate the high quality of the ferroelectric nanostructures (Fig. 3a,d), despite the low volume of the ferroelectric material. To the best of our knowledge, the present capacitors of about 60 nm diameter and 20–40 nm height are the smallest fully processed ferroelectric capacitors to be created. In contrast to previous work[5], the structures are individually addressable, as is shown in Fig. 3g,h, where two neighbouring nanocapacitors have been switched into opposite states. Pt/PZT/Pt nanocapacitors exhibited a fairly uniform piezoelectric response over a large area (see Supplementary Information, Fig. S6). For areas of limited size (see Supplementary Information, Fig. S7), the standard deviation of the coercive voltage was less than 10%. Retention

© 2008 Macmillan Publishers Limited. All rights reserved.

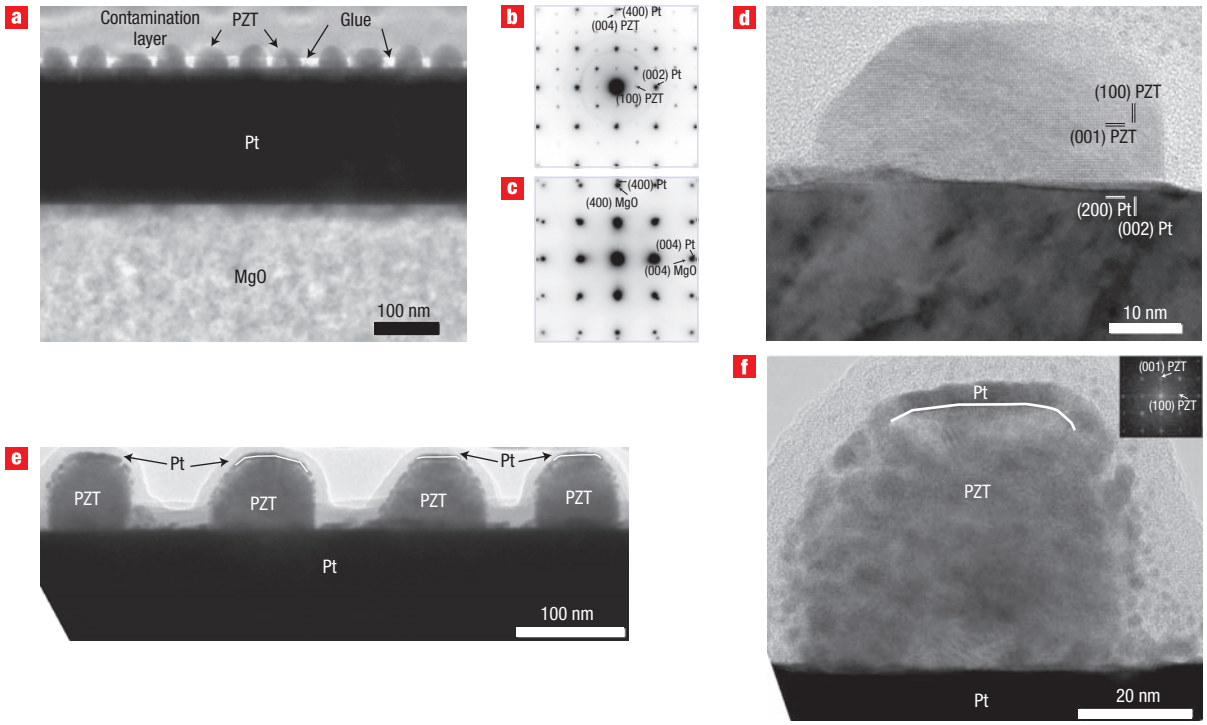

Figure 2 MFM nanocapacitor. a, Cross-sectional TEM image of epitaxial PZT nanoislands on Pt/MgO(100). The TEM sample was prepared by standard methods of mechanical polishing and ion milling. The contamination layer originates from the ion beam thinning process, in which tungsten from the sample holder is deposited onto the upper surface of the glue layer due to the ion beam hitting a small part of the sample holder; the area close to the platinum surface is protected by the sample edge, resulting in the bright undeposited glue region. **b**,**c**, Electron diffraction patterns obtained at the interfaces of PZT/Pt(100) and Pt/MgO(100), respectively. **d**, HRTEM image of PZT/Pt/MgO(100). **e**, Cross-sectional TEM micrograph of the Pt/PZT/Pt nanocapacitor on a MgO(100) substrate (substrate not shown here). The sample was prepared using the FIB technique. **f**, HRTEM image of one MFM nanocapacitor. The inset shows a fast Fourier transform image of the PZT island. The white lines in **e** and **f** mark the interface between Pt and PZT. Nanoparticles decorating the PZT nanostructures and the amorphous layer on the PZT are due to FIB sample preparation.

measurements showed that the present nanocapacitors also ensure long-term stability of polarization for more than 74 h (see Supplementary Information, Fig. S7). The preparation of Pt/PZT/Pt nanocapacitors has been performed here as a proof of principle. If particularly good fatigue properties are required, it should be possible to replace the Pt electrodes with oxide electrodes such as IrO_2, or even replace PZT by a fatigue-free material, for example, rare-earth-substituted bismuth titanate.

The large area of the array and the high quality of the epitaxial nanostructures will enable comprehensive in-depth investigations of structures and properties. In order to gain insight into the origin of the excellent ferroelectric properties of the samples, the domain structure in as-grown nano-sized PZT islands was characterized using high-resolution synchrotron X-ray diffraction. It was confirmed that as-deposited PZT nanoislands were grown epitaxially (Fig. 4a,b) with a high tetragonality (that is, $c/a \sim 1.048$ for Pt/MgO(100) and 1.061 for Nb-doped STO(100)). X-ray diffraction contour mapping of the *HK* and *HL* reciprocal space on PZT(001) plane reflection revealed that the PZT nanoislands with ~75-nm lateral size are characterized by multi-a/c domain structures, consisting of a major fraction of c-domains and a minor fraction of a-domains (Fig. 4c–e). Unlike for the case of a continuous film or a self-assembled nanostructure, where the [001] axes of the a-domains are tilted by an angle $\Delta\omega$ with respect to the substrate plane to maintain the a/c twin boundary coherence[18], as-grown discrete PZT nanoislands exhibit non-tilted a-domains (that is, $\Delta\omega = 0$), whose [001] axes are aligned parallel to the plane of the underlying substrate (that is, Pt/MgO(100)) (Fig. 4d; see also Supplementary Information, Fig. S8, for a schematic illustration). This striking observation is in line with a recent experimental finding from 100-nm-sized $PbTiO_3$ patterns on Pt/MgO(100), and can be attributed to a rather high degree of misfit strain relaxation in nanometre-sized ferroelectric islands[19]. The evolution of non-tilted a-domains was also observed for epitaxial PZT nanoislands grown on Nb-doped STO(100) (see Supplementary Information, Fig. S9). Further in-depth investigations using switching spectroscopy PFM (SS-PFM)[20] will shed more light on the role of a/c-domains in these nanostructures.

In general, ferroelastic domains are known to be strongly clamped by the substrate, and thus piezoresponse is limited for the case of a continuous ferroelectric film. However, it has also been reported that such unfavourable substrate clamping could be significantly reduced and domain switching could be triggered due to the reduced misfit strain, when a film is patterned into discrete islands[21,22]. Here, we could observe reduced clamping and the presence of domain switching in epitaxially grown PZT nanoislands during piezoelectric hysteresis measurements; a high d_{33} (up to 120 pm V^{-1}) was observed during a first hysteresis run, and it decreased to 100 pm V^{-1} during the second hysteresis run due to the elimination of mobile 90° domains under the electric field. The presence of a/c-domains in the nanostructures, as proven by synchrotron X-ray diffraction, is a sign of the very low level of strain in the nanostructures[23].

© 2008 Macmillan Publishers Limited. All rights reserved.

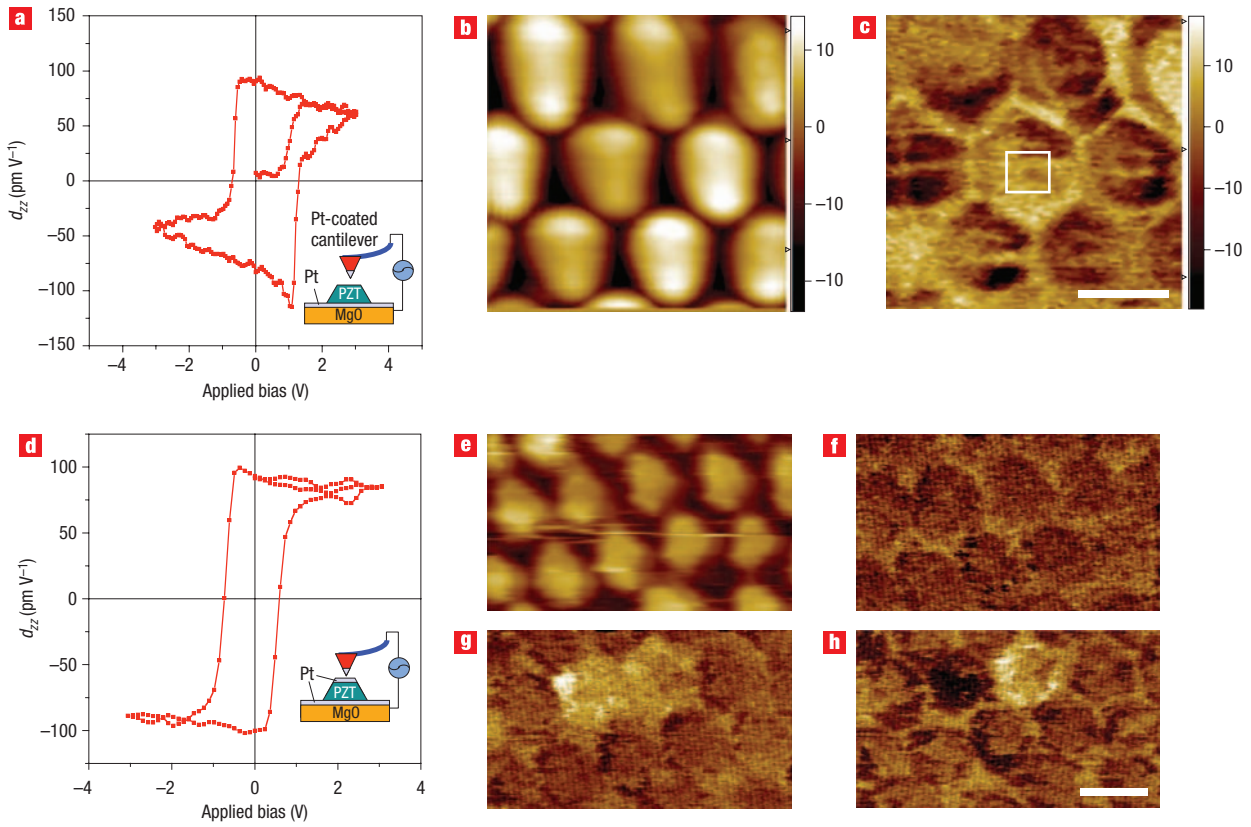

Figure 3 Ferroelectric properties. a, Piezoelectric hysteresis loop obtained from epitaxially grown PZT on a Pt/MgO(100) substrate. **b**,**c**, Topographic (**b**) and piezoresponse (**c**) images of nanoisland PZT/Pt/MgO(100). The hysteresis loop shown in **a** was obtained from the area marked by a white rectangle in **c.** **d**, Piezoelectric hysteresis loop obtained from a ferroelectric (Pt/PZT/Pt/MgO(100)) nanocapacitor. **e**, Topographic image of the corresponding sample. **f**–**h**, PFM images before switching (**f**), after positive switching of two capacitors by applying $+3V_{dc}$ (**g**), and after negative switching of one of the two previously switched capacitors by applying $-3V_{dc}$ (**h**). Insets in **a** and **d** represent the measurement configuration. The scale bars in **b**,**c** and **e**–**h** are 100 nm.

In summary, well-ordered large-area 2D arrays of epitaxial $Pb(Zr_{0.20}Ti_{0.80})O_3$ (PZT) nanoislands were obtained on either Nb-doped $SrTiO_3$(100) or Pt/MgO(100) substrates by PLD at an elevated growth temperature (650 °C) by using ultrathin AAO membranes as shadow masks, taking advantage of the excellent thermal stability of this ceramic stencil material. We also established novel ferroelectric nanocapacitor arrays that are individually addressable for nonvolatile ferroelectric random access memory (FeRAM) devices with near Tb inch^{-2} density.

METHODS

PREPARATION OF ULTRATHIN ANODIC ALUMINIUM OXIDE

Ultrathin AAO membranes were prepared by a two-step anodization of surface-finished aluminium[24]. After the second anodization, a thin layer of polystyrene (PS) film was spin-coated on the surface of the AAO membrane at 3,000 r.p.m. for 1 min using a 1.4 wt% PS/$CHCl_3$ solution, and heated to 80 °C to evaporate the solvent (see Supplementary Information, Fig. S2). Afterwards, the aluminium substrate was removed by floating the sample onto the surface of an acid mixture of $CuCl_2$ and HCl. The thin PS layer plays an important role in the handling of the ultrathin AAO mask. It prevents the ultrathin ceramic membrane from undergoing mechanical deformations, such as folding, cracking or ripping. After complete removal of the aluminium, the resulting sample was rinsed with HNO_3 solution in order to remove undesired solid copper that was deposited during the aluminium removal process. The resulting ultrathin AAO/PS composite film remained floating on the surface of the solution because of the hydrophobic nature of PS. The barrier layer at the bottom of pores could be selectively removed by placing the composite film on the surface of a 5 wt% H_3PO_4 solution at 30 °C for 15 min for AAO masks formed under 25 V, and for 30 min for AAO masks formed under 40 V. Because the pore walls are protected by the PS film, it is possible to achieve selective etching of the barrier layer without affecting the pore diameter. The ultrathin AAO membrane (typical lateral dimension >2 cm^2) was transferred onto the desired substrate, and then immersed in $CHCl_3$. This process enabled us to completely remove PS from the oxide membrane. (Alternatively, oxygen plasma treatment could be used for the removal of the PS.) The ultrathin AAO mask exhibited excellent contact with the substrate and could not be removed even under a strong stream of nitrogen gas.

PULSED LASER DEPOSITION

PLD was performed at high substrate temperatures, generally exceeding 450 °C, ablating a ceramic target with 10% PbO excess using a KrF excimer laser ($\lambda = 248$ nm) operated at an energy fluence of 400 mJ cm^{-2} and a repetition rate of 10 Hz. PLD was performed in a low oxygen pressure of 1×10^{-6} torr. Self-ordered anodic AAO was used as the stencil mask (which can conveniently be fabricated by conventional anodization processes)[24,25]. In a typical anodization, a perfect honeycomb-like structure of self-ordered arrays of oxide nanopores is formed within domains with a scale of a few micrometres. Accordingly, arrays of ferroelectric nanocapacitors fabricated from an oxide mask are short-range ordered, and might be far from ideal for real-life storage applications. Although we are reporting self-ordered patterns in the present work, long-range ordered arrays of ferroelectric nanocapacitors can also be realized by extending our generic approach. Fabrication of long-range ordered AAO with tunable pore densities has already been established by our group and others[26–30]. Wafer-scale fabrication of ideally ordered AAOs with square or

© 2008 Macmillan Publishers Limited. All rights reserved.

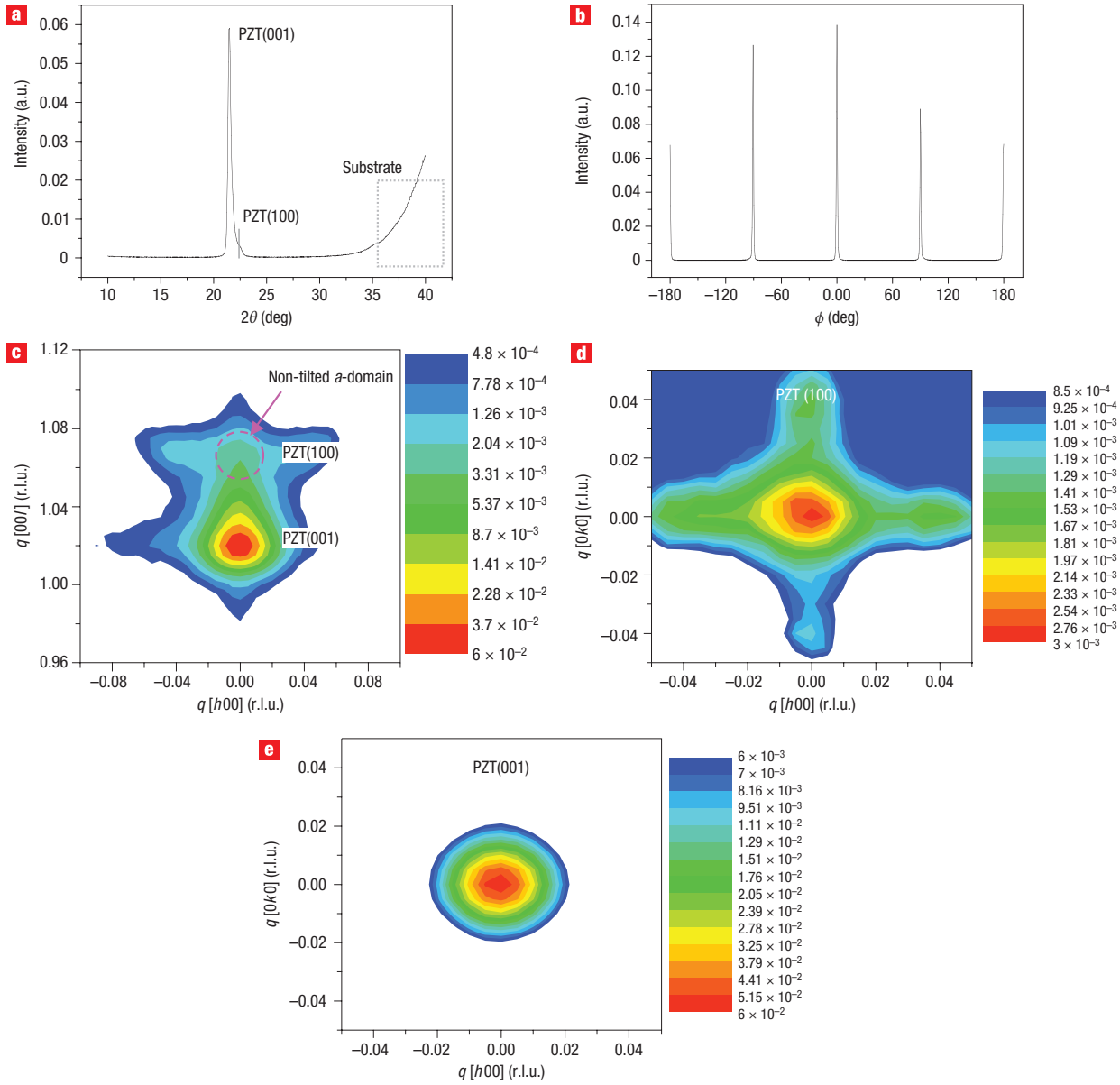

Figure 4 High-resolution X-ray diffraction patterns of epitaxial PZT nanoislands grown on Pt/MgO(100). a, The broad spectral feature highlighted by the rectangle in this 2θ scan is due to the Pt/MgO(100) substrate. **b**, PZT(101)-Φ scan. Reciprocal space mapping of the sample. **c**, HL scan of PZT(001). **d**, HK scan of PZT(100) manifesting the evolution of non-tilted *a*-domains, whose [001] axes are parallel to the substrate plane. **e**, HK scan of PZT(001). In panels **c**–**e**, r.l.u. indicates reciprocal lattice units.

hexagonal arrays of nanopores has also been demonstrated by combining anodization processes with nanoimprinting techniques[26]. The resulting AAOs can be used as a hard mask for generating arrays of ferroelectric nanocapacitors that are compatible with memory applications.

PIEZOELECTRIC SCANNING FORCE MICROSCOPY

PFM was performed using a CP-Research atomic force microscope (AFM, VEECO) working in contact mode. The piezoresponse signal was measured using a conducting AFM tip (ATEC-FM, Nanosensors) with an elastic constant of about 2.5 N m and a lock-in amplifier (DSP7260, Signal Recovery). The a.c. probing signal of about 25 kHz was set to about half of the coercive voltage (0.4 V_{pp}), and for hysteresis measurements a d.c. voltage was superimposed[31].

TRANSMISSION ELECTRON MICROSCOPY

Conventional TEM investigations were carried out using a Philips CM 20 Twin microscope, and HRTEM investigations were performed using a Jeol 4010 microscope. Some of the thin samples for TEM investigations were prepared by standard methods of mechanical polishing and ion milling. The other samples were prepared by FIB milling using a gallium ion beam in an FEI Nova 600 NanoLab system.

SYNCHROTRON X-RAY DIFFRACTION

Domain structures in nanometre-sized ferroelectric islands were characterized by an *in situ* high-resolution synchrotron X-ray diffraction installed on the Huber six-circle diffractometer of the 3C2 and 10C1 synchrotron X-ray diffraction beam line at the Pohang Light Source (PLS). The beam size at the focal point was typically less than 1 mm^2. A scintillation detector was used to record the diffracted beam intensities. Complete structural characterization was carried out by performing 2D *HKL*-mesh scans in reciprocal space for $Pb(Zr_{0.20}Ti_{0.80})O_3$ (001) and (100) reflections.

Received 10 March 2008; accepted 9 May 2008; published 15 June 2008.

© 2008 Macmillan Publishers Limited. All rights reserved.

References

1. Auciello, O., Scott, J. F. & Ramesh, R. The physics of ferroelectric memories. *Phys. Today* **51,** 22–27 (July 1998).
2. Cheong, S.-W. & Mostovoy, M. Multiferroics: a magnetic twist for ferroelectricity. *Nature Mater.* **6,** 13–20 (2007).
3. Cho, Y. Nanoscale ferroelectric information storage based on scanning nonlinear dielectric microscopy. *J. Nanosci. Nanotechnol.* **7,** 105–116 (2007).
4. Cross, L. E. *Ferroelectric Ceramics* (ed. Setter, N.) 1–85 (Birkhäuser, Basel, 1993).
5. Evans, P. R. *et al.* Toward self-assembled ferroelectric random access memories: Hard-wired switching capacitor arrays with almost Tb/in.^{2} densities. *Nano Lett.* **7,** 1134–1137 (2007).
6. Alexe, M., Harnagea, C., Hesse, D. & Gösele, U. Polarization imprint and size effects in mesoscopic ferroelectric structures. *Appl. Phys. Lett.* **70,** 242–244 (2001).
7. Bühlmann, S., Dwir, B., Baborowski, J. & Muralt, P. Size effect in mesoscopic epitaxial ferroelectric structures: Increase of piezoelectric response with decreasing feature size. *Appl. Phys. Lett.* **80,** 3195–3197 (2002).
8. Ganpule, C. S. *et al.* Scaling of ferroelectric and piezoelectric properties in $Pt/SrBi_2Ta_2O_9/Pt$ thin films. *Appl. Phys. Lett.* **75,** 3874–3876 (1999).
9. Stanishevsky, A. *et al.* Radiation damage and its recovery in focused ion beam fabricated ferroelectric capacitors. *J. Appl. Phys.* **92,** 3275–3278 (2002).
10. Ahn, C. H. *et al.* Local, nonvolatile electronic writing of epitaxial $Pb(Zr_{0.52}Ti_{0.48})O_3/SrRuO_3$ heterostructures. *Science* **276,** 1100–1103 (1997).
11. Gruverman, A., Auciello, O. & Tokumoto, H. Imaging and control of domain structures in ferroelectric thin films via scanning force microscopy. *Annu. Rev. Mater. Sci.* **28,** 101–123 (1998).
12. Cho, Y., Hashimoto, S., Odagawa, N., Tanaka, K. & Hiranaga, Y. Nanodomain manipulation for ultrahigh density ferroelectric data storage. *Nanotechnology* **17,** S137–S141 (2006).
13. Kalinin, S. V. *et al.* Intrinsic single-domain switching in ferroelectric materials on a nearly ideal surface. *Proc. Natl Acad. Sci. USA* **104,** 20204–20209 (2007).
14. Odagawa, N. & Cho, Y. Wall behavior of nanodomains as a function of their initial state. *Appl. Phys. Lett.* **89,** 192906 (2006).
15. Torii, K. *et al.* Fabrication and properties of one-mask-patterned ferroelectric integrated capacitors. *Electr. Eng. Jpn.* **121,** 43–50 (1997).
16. Lee, S.-K. *et al.* Well-ordered large-area arrays of epitaxial ferroelectric $(Bi,La)_4Ti_3O_{12}$ nanostructures fabricated by gold nanotube-membrane lithography. *Appl. Phys. Lett.* **86,** 152906 (2005).
17. Lee, W., Alexe, M., Nielsch, K. & Gösele, U. Metal membranes with hierarchically organized nanotube arrays. *Chem. Mater.* **17,** 3325–3327 (2005).
18. Chu, M.-W., Szafraniak, I., Hesse, D., Alexe, M. & Gösele, U. Elastic coupling between 90 ° twin walls and interfacial dislocations in epitaxial ferroelectric perovskites: A quantitative high-resolution transmission electron microscopy study. *Phys. Rev. B* **72,** 174112 (2005).
19. Lee, K., Yi, H., Park, W.-H., Kim, Y. K. & Baik, S. Lateral size effects on domain structure in epitaxial $PbTiO_3$ thin films. *J. Appl. Phys.* **100,** 051615 (2006).
20. Jesse, S. *et al.* Direct imaging of the spatial and energy distribution of nucleation centers in ferroelectric materials. *Nature Mater.* **7,** 209–215 (2008).
21. Lee, K., Kim, K., Kwon, S.-J. & Baik, S. Two-dimensional planar size effects in epitaxial $PbTiO_3$ thin films. *Appl. Phys. Lett.* **85,** 4711–4713 (2004).
22. Nagarajan, V. *et al.* Dynamics of ferroelastic domains in ferroelectric thin films. *Nature Mater.* **2,** 43–47 (2002).
23. Speck, J. S. & Pompe, W. Domain configurations due to multiple misfit relaxation mechanisms in epitaxial ferroelectric thin films. I. Theory. *J. Appl. Phys.* **76,** 466–476 (1994).
24. Masuda, H. & Fukuda, K. Ordered metal nanohole arrays made by a two-step replication of honeycomb structures of anodic alumina. *Science* **268,** 1466–1468 (1995).
25. Li, A. P., Müller, F., Birner, A., Nielsch, K. & Gösele, U. Hexagonal pore arrays with a 50–420 nm interpore distance formed by self-organization in anodic alumina. *J. Appl. Phys.* **84,** 6023–6026 (1998).
26. Lee, W., Ji, R., Ross, C. A., Gösele, U. & Nielsch, K. Wafer-scale Ni imprint stamps for porous alumina membranes based on interference lithography. *Small* **2,** 978–982 (2006).
27. Choi, J., Nielsch, K., Reiche, R., Wehrspohn, R. B. & Gösele, U. Fabrication of monodomain alumina pore arrays with an interpore distance smaller than the lattice constant of the imprint stamp. *J. Vac. Sci. Technol. B* **21,** 763–766 (2003).
28. Sun, Z. & Kim, H. K. Growth of ordered, single-domain, alumina nanopore arrays with holographically patterned aluminum films. *Appl. Phys. Lett.* **81,** 3458–3460 (2002).
29. Masuda, H., Yamada, H., Satoh, M. & Asoh, H. Highly ordered nanochannel-array architecture in anodic alumina. *Appl. Phys. Lett.* **71,** 2770–2772 (1997).
30. Lee, W., Ji, R., Gösele, U. & Nielsch, K. Fast fabrication of long-range ordered porous alumina membranes by hard anodization. *Nature Mater.* **5,** 741–747 (2006).
31. Harnagea, C., Pignolet, A., Alexe, M. & Hesse, D. Piezoresponse scanning force microscopy: What quantitative information can we really get out of piezoresponse measurements on ferroelectric thin films. *Intergr. Ferroelectr.* **44,** 113–124 (2002).

Supplementary Information accompanies this paper at www.nature.com/naturenanotechnology.

Acknowledgements

H. Han is grateful for the award of a fellowship of the German Academic Exchange Service (DAAD) and for support by DFG and KRF. Financial support from the Volkswagen Foundation (Project I/80897) and partly from the Brain Korea 21 Program is also acknowledged. We are thankful to S. Swatek and N. Schammelt for TEM sample preparation. We also thank R. Hillebrand for discussions on statistical analyses for the size distribution and 2D ordering of ferroelectric nanocapacitors.

Author information

Reprints and permission information is available online at http://npg.nature.com/reprintsandpermissions/.
Correspondence and requests for materials should be addressed to W.L.

© 2008 Macmillan Publishers Limited. All rights reserved.